FABRICATION OF MAGNETIC BIOACTIVE GLASS NANOPARTICLES

A THESIS SUBMITTED TO
THE GRADUATE SCHOOL OF NATURAL AND APPLIED SCIENCES
OF
MIDDLE EAST TECHNICAL UNIVERSITY

BY

CANSU TAŞAR

IN PARTIAL FULFILLMENT OF THE REQUIREMENTS
FOR
THE DEGREE OF MASTER OF SCIENCE
IN
METALLURGICAL AND MATERIALS ENGINEERING

AUGUST 2022

Approval of the thesis:

FABRICATION OF MAGNETIC BIOACTIVE GLASS NANOPARTICLES

submitted by **CANSU TAŞAR** in partial fulfillment of the requirements for the degree of **Master of Science** i**n Metallurgical and Materials Engineering, Middle East Technical University** by,

Prof. Dr. Halil Kalıpçılar
Dean, Graduate School of **Natural and Applied Sciences** _____

Prof. Dr. Ali Kalkanlı
Head of the Department, **Metallurgical and Materials Engineering** _____

Assoc. Prof. Dr. Batur Ercan
Supervisor, **Metallurgical and Materials Engineering, METU** _____

Examining Committee Members:

Prof. Dr. Abdullah Öztürk
Metallurgical and Materials Eng, METU _____

Assoc. Prof. Dr. Batur Ercan
Metallurgical and Materials Engineering,METU _____

Assoc. Prof. Dr. Erhan Bat
Chemical Eng, METU _____

Asst. Prof. Dr. Cem Bayram
Nanotechnology and Nanomedicine, Hacettepe University _____

Asst. Prof. Dr. Yusuf Keleştemur
Metallurgical and Materials Eng., METU _____

Date: 18.08.2022

I hereby declare that all information in this document has been obtained and presented in accordance with academic rules and ethical conduct. I also declare that, as required by these rules and conduct, I have fully cited and referenced all material and results that are not original to this work.

Name, Surname: Cansu Taşar

Signature :

ABSTRACT

FABRICATION OF MAGNETIC BIOACTIVE GLASS NANOPARTICLES

Taşar,Cansu
Master of Science, Metallurgical and Materials Engineering
Supervisor: Assoc. Prof. Batur Ercan

August 2022, 54 pages

Different compositions of bioactive glass nanoparticles have been investigated for various applications, including cancer treatment, drug delivery, bone regeneration, etc. However, targeting of bioactive glass nanoparticles to desired tissues still remains to be a challenge. In this research, sol-gel synthesized bioactive glass and superparamagnetic iron oxide nanoparticles (SPIONs) were combined using two different approaches to obtain magnetic bioactive glass nanoparticle composites. In the first approach SPIONs were embedded into the bioactive glass nanoparticles (SEBG), and in the second approach SPIONs were deposited onto them as a thin shell (SDBG). The dimensions of the nanoparticles were calculated to be 180±9 and 420±10nm for SEBG and SDBG, respectively. The magnetizations of the nanoparticles were measured to be 4 and 9 emu/g for SEBG and SDBG, respectively. *In vitro* bioactivity experiments showed hydroxyapatite formation on both nanoparticles after soaking them in simulated body fluid (SBF) for 14 days. Additionally, bone cells proliferated and remained viable up to 7 days of culture *in vitro* upon their interaction with SEBG and SDBG nanoparticles. Similar viability results were also observed once experiments were carried out in the presence of 0.4T external static magnetic field to better mimic cellular response under magnetic

targeting. Cumulatively, these results demonstrated that the synthesized magnetic bioactive glass nanoparticles were superparamagnetic, promoted bone cell viability independent of the presence of magnetic field and exhibited bioactive properties.

Keywords: Bioactive glass, SPION, sol-gel, bone cells, bioactivity

ÖZ

MANYETİK BİYOAKTİF CAM NANOPARTİKÜLLERİNİN ÜRETİMİ

Taşar,Cansu
Yüksek Lisans, Metalurji ve Malzeme Mühendisliği
Tez Yöneticisi: Doç. Dr. Batur Ercan

Ağustos 2022, 54 sayfa

Cam yüzeyi ile dokular arasında bağ oluşturma yetenekleri nedeniyle son yılda farklı biyoaktif cam kompozisyonları incelenmiştir. Biyoaktif cam, kanser tedavisi, hedefe yönelik terapiler ve kemik tedavisi dahil olmak üzere çeşitli uygulamalar için önerilmiştir, ancak biyoaktif cam parçacıklarının istenen dokulara hedeflenmesi zordur. Bu araştırmada, manyetik biyoaktif cam nanoparçacıklar elde etmek için biyoaktif sentezlenen sol-jel ile süperparamanyetik demir oksit nanoparçacıkları (SPIONlar) birleştirilmiştir. İki farklı nanoparçacık üretilmiştir. SPIONlar ya biyoaktif cam nanoparçacıklara (SEBG) gömülmüş ya da ince bir kabuk (SDBG) olarak üzerlerine yerleştirilmiştir. Nanopartiküllerin boyutları SEBG ve SDBG için sırasıyla 180±9 ve 420±10 nm olarak hesaplanmıştır. Nanopartiküllerin manyetizasyonları SEBG ve SDBG için sırasıyla 4 ve 9 emu/g olarak ölçülmüştür. Nanopartiküllerin in vitro biyoaktivitesi, simüle edilmiş vücut sıvısında (SBF) 14 gün boyunca bekletilerek değerlendirilmiş ve sonuçlar, her iki nanopartikülde de hidroksiapatit oluşumunu göstermiştir. Ek olarak, kemik hücreleri SEBG ve SDBG nanopartikülleri ile etkileşime girdiklerinde başarılı bir şekilde çoğalmış ve in vitro kültürde 7 güne kadar canlılığını korumuştur. Benzer canlılık sonuçları, manyetik stimülasyon altında hücresel yanıtı daha iyi taklit etmek için 0.4T harici statik

manyetik alan altında deneyler tamamlandıktan sonra da gözlenmiştir. Kümülatif olarak, bu sonuçlar sentezlenen manyetik biyoaktif cam nanoparçacıkların süperparamanyetik olduğunu, biyoaktif özellikler sergilediğini ve in vitro kemik hücrelerinin canlılığını manyetik alandan bağımsız olarak desteklediğini göstermektedir.

Anahtar Kelimeler: Biyoaktif cam, SPION, sol-jel, kemik hücreleri, biyoaktivite

To all who support and compass…

ACKNOWLEDGMENTS

The Turkish Scientific Research Council (TÜBITAK) funded this research, Grant No 117M187, 118M652 and 219M480.

Primarily, I would like to thank my advisor, Assoc. Prof. Dr. Batur Ercan, for his guidance and assistance, direction, and encouragement for both my thesis and daily life pieces of advice. During my master's degree, he constantly shares his experience and knowledge with me. He encouraged me to keep going. Therefore, I consider myself truly fortunate to work with him. It would be hard for me to finish my thesis without his assistance.

I'd also like to thank my laboratory mates, notably Melisa Kafalı, Yağmur Göçtü, and Alper Haliloğlu, for their support and help. Melisa Kafalı, for the time and support you gave me, I think few people can show this patience. We became close friends quickly and it was a great chance to have friendship and endless support anytime. I will always be grateful to you.

I am grateful to all METU Metallurgical and Materials Engineering Department and METU Center Lab members that assisted me with my analysis. I'd like to offer my heartfelt appreciation to the Center of Excellence in Biomaterials and Tissue Engineering (BIOMATEN)

TABLE OF CONTENTS

LIST OF TABLES

TABLES

LIST OF FIGURES

FIGURES

LIST OF ABBREVIATIONS

ABBREVIATIONS

BG	BIOACTIVE GLASS
SPION	SUPER PARAMAGNETIC IRON OXIDE
SEBG	SPION EMBEDDED BIOACTIVE GLASS NANOPARTICLES
SDBG	SPION DEPOSITED BIOACTIVE GLASS NANOPARTICLES

CHAPTER 1

INTRODUCTION

Since Hench's discovery [1,4–6], bioactive glass (BG) [1,2] has been used for a range of purposes, including bone grafting, spinal issues, and nerve injury. The most common network former used in BG is silicon dioxide (SiO_2). Bioactivity and biocompatibility are the two main characteristics of bioactive glasses. The formation of the hydroxyapatite (HA) layer, which is due to ion dissolution form BG, is typically the reason for the bioactivity of a glass system [6–9].

Bioactive glasses are surface-reactive glass-ceramic materials. Plus, they have unique qualities, including osteoconductivity, biodegradability, and cellular support. Therefore, bioactive glasses have several different applications [10]. These applications include drug delivery, targeted therapies cancer treatments and hyperthermia. Magnetic bioactive glasses would be candidate materials for the treatment of several diseases because they combine both bioactivity and magnetic properties [10–13].

Although there are several methods for creating magnetic bioactive glass nanoparticles, the sol-gel technique is promising due to its lower temperature requirement, which would prevent loss of magnetic properties while providing particle size control. Iron oxides have several phases, but magnetite (Fe_3O_4) is one of the common phase utilized for biomedical applications due to its improved magnetization compared to other iron oxide forms [14,15]. Additionally, below a certain size, they become superparamagnetic. Consequently, they do not have any remnant magnetization after magnetization is removed from the system. Since superparamagnetic iron oxide particles (SPIONs) do not retain their magnetic properties when the magnetic field is withdrawn, they are one of the popular

magnetic nanoparticles employed in biomedical applications. Thus, they become a candidate material for several different biomedical applications.

Fabrication of magnetic bioactive glasses is primarily used to combine magnetic and biocompatible features, as the name suggests [16–18]. Numerous research has attempted to explain this topic to provide clarity. [14,19–21]. Briefly, by the help of magnetic field magnetic bioactive glasses can effectively be utilized for cancer treatment, hyperthermia, and drug delivery. Besides, bioactive glass could provide fast regeneration or healing. Therefore, this document was created to give a thorough understanding of magnetic bioactive glasses closely.

1.1 Objective

The aim of the project was defined as synthesizing magnetic bioactive glass nanoparticles while preserving their superparamagnetic properties. Additionally, assessment of their biological properties for potential orthopedic applications. Briefly, this work provides a discussion of the pertinent figures of magnetic bioactive glasses. Due to their biocompatibility and minimal rejection in the body, magnetic bioactive glasses are an excellent choice for various biomedical applications. Experiments with magnetic bioactive glasses are conducted to provide precise explanations of glass systems.

1.2 Thesis Outline

Introduction part includes all primary objectives and the aim of the thesis. This thesis is divided into five chapters, the first part which introduces magnetic bioactive glasses and discusses regenerative bioactive materials as well as magnetic bioactive glasses.

The literature review part of the study is covered in Chapter 2. Fundamental characteristics of magnetic bioactive glasses are detailed in this chapter. The description of magnetic bioactive glasses and basic fabrication methods are provided. Additionally, several studies related to the magnetic bioactive glasses are given.

The materials and method part are included in Chapter 3. All chemicals with their grade, each method for magnetic bioactive glass nanoparticles and biological experiments are described in detail.

Chapter 4 begins with materials characterization techniques. Additionally, all characterization, bioactivity and 3-(4,5-dimethyl-2-thiazolyl)-2,5-diphenyl-2H-tetrazolium bromide (MTT) assay results are also given in Chapter 5. Besides, discussions of material synthesis, bioactivity, and cellular are also included in this section.

Based on this thesis, more work is suggested according to the investigations and the discussions around the synthesized nanoparticles, conclusion and future work which is included in Chapter 6.

CHAPTER 2

LITERATURE REVIEW

Biomaterials could be described as materials interacting with biological systems and they have been employed in a controlled manner for over fifty years. Since perspective of bioactive materials has changed significantly, both materials and production methods altered with time. [21,24].

Depending on the biological response, biomaterials are categorized into three different groups. First-generation biomaterials, such as stainless steel, was preferred as they were inert, meaning they had weak interactions with living tissues. Then, second-generation biomaterials were developed that have beneficial effects on the body. The second-generation biomaterials had better interactions with living tissues and the concept of bioactivity emerged. The third-generation biomaterials healed damaged tissue parts and the concept of tissue engineering emerged.

In summary, magnetic bioactive glass presented the most distinguishing feature of third-generation biomaterials [8, 10, 25–27]. Many modern medical applications in tissue engineering rely on the bioactivity mechanism, in which living tissues adhere to and integrate with an artificial implant through stable chemical bonds. Efficient bonding and bioactive fixation are still necessary for bioactive glass criteria to provide bone formation [4-17].

After Hench's discovery in 1969, bioactive glass was employed in several applications and it has contiously evolved. Many commercial and clinical products are now routinely utilized in patients two of them were given in Figure. 2.1.

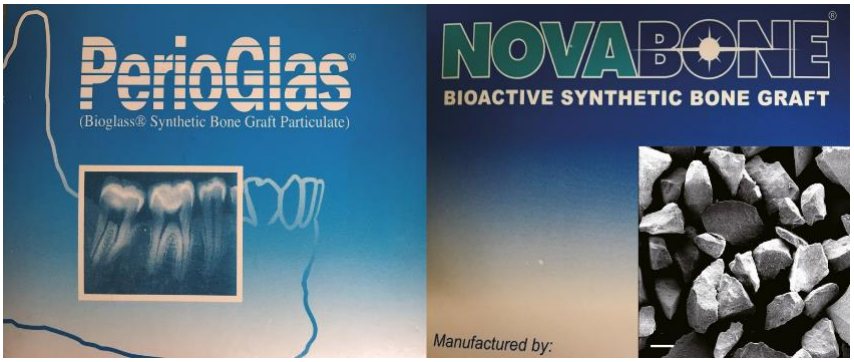

Figure 2.1. PerioGlas® and NovaBone® [1]

Silicon dioxide (or silicate) and three other key components, such as sodium dioxide, calcium oxide, and phosphorus, are the most critical components of bioactive glasses. With the help of silica, oxide network of glass structure was created by the tetrahedral structure of silica. Glass modifiers, network formers or intermediates could be provided in different variations into this structure to change the glass network. Changes in glass compositions helped glass scientists to improve numerous formulations of bioactive glasses [31,32]. Thus, new bioactive glass products could be produced depending on the application requirements. Common bioactive glass compotions were given in table 2.1. New products were produced according to the desired degradation rate and/or the therapeutic effects in the glass structure. In short, although different compositional designs are possible, it may be more explanatory to give the frequently used bioglass compositions.

Table 2.1. Common silica based bioactive glass compositions. (wt%) [2]

COMPONENT	45S5	58S	70S30C	S53P4	77S
SiO_2	45	58	70	53	77
Na_2O	24.5	-	-	23	-
P_2O_5	6	9	-	4	9
CaO	24.5	33	30	20	14

The creation of a hydroxyapatite (HCA) layer [3,33], which is mainly connected with ion dissolution from the glass surfaces, is often used to explain the bioactivity of a glass system. As the HCA the layer is very similar to the mineral phase of natural bone, it could promote new bone formation. Plus, it provides therapeutic ion dissolution with the help of rapid reactions on the glass surfaces [34]. Morover, studies have shown that HCA layer can be formed around 8-10 h and its thickness increases with time. Similarly, while the HCA layer formation time may vary depending on the composition and production method, the process of HCA layer formation on the entire glass surface can be explained with the similar chemical reactions [1,22].

Figure. 2.3 depicts schematic representation of HCA layer creation on a glass surface. The bone-bonding mechanism (or HCA layer formation mechanism) starts with the release of several ions (Ca^{+2}, Na^{+}) from the glass surface when glass is exposed to body fluid. Once silica-rich layer forms and the pH increases with silanol groups, Si-O-Si bonds are broken. Then, Ca^{+2} and PO_4^{-3} migrate to the glass surface. Afterwards, the CaO-P_2O_5 layer forms on the glass surface and crystalizes with OH^- and CO_3^{-2} layers [35].

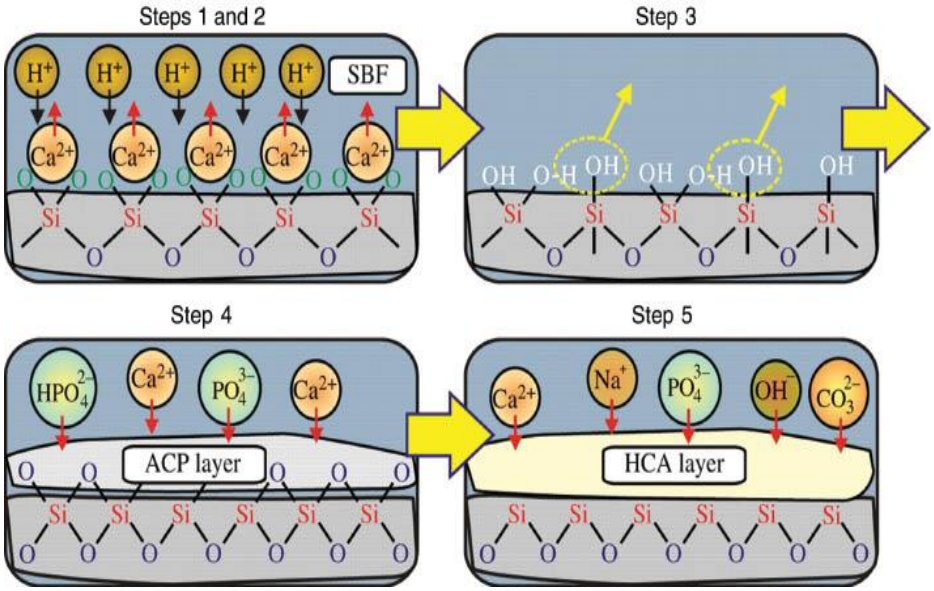

Figure 2.2. Hydroxycarbonate apatite (HCA) formation steps on bioactive glass [3]

The bioactivity of glass is strongly connected to the bioactive glass composition. For example, according to Yousefi et al. [3], the Ca/P ratio is one of the primary characteristics that alter bioactivity by substantially changing HCA layer formation and dissolution rate. Since its development, bioactive glasses were fabricated using melt-quenching method and this technique has certain drawbacks, such as high energy consumption, low purity, and process control. Due to its homogeneity, uniformity, and low-temperature synthesis, the sol-gel approach has recently become one of the most commonly-used technique for producing bioactive glasses [23,36–38]. Other processes, including spray drying and drawing, are still being used to improve the product quality. In Figure 2.3, SEM images of several glass products were provided to highlight the product diversity depending on the glass production technique. Since BG products and particle morphologies significantly differ depending on the fabrication method, the propeties of the bioactive glasses change dramatically, as well. For instance, size and morplogy control could chage the response of BGs in biological environments. Briefly, new production strategies could be developed for BG product needs.

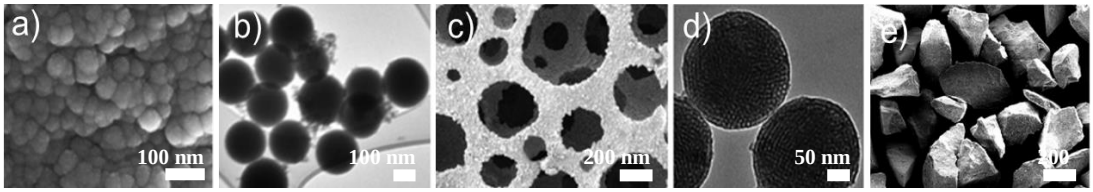

Figure 2.3. SEM images of bioactive sol–gel BG produced under a) acid catalysis, b) base catalysis and c) gel-cast foamed BG. d) TEM image of ordered mesoporous BG and e) SEM image of Novabone®. Scale bars are a) 100 nm, b) 100 nm, c) 200 μm, d) 50 nm, e) 200 μm [4]

As the name implied, magnetic bioactive glasses also belonged to the bioactive glass class. To achieve magnetization, most researcher incorporated iron oxide to bioactive glass using different approaches. Due to various distinct benefits iron oxide nanoparticles have to offer, these particles are used in several applications (e.g., cancer treatments, drug delivery applications) [23]. They exhibit excellent magnetic, catalytic, and biological capabilities. For iron oxide particles, the nature of magnetism varies depending on the order of Fe^{+3} and Fe^{+2} ions within the crystal [24,25].

Magnetite (Fe_3O_4) was the preferable option among these phases due to its higher magneticzation. Furthermore, iron oxide nanoparticles (magnetite and maghemite) below a specific size transform into superparamagnetic iron oxide particles (SPIONs), which have no remnant magnetization when magnetization is removed from the system. As a result, as the size of nanoparticles reduces, their application areas expand. All the detailed magnetization effect on iron oxides were summarized in Figure 2.4. Besides, responses depending on the size and magnetic moment alignment were given closely.

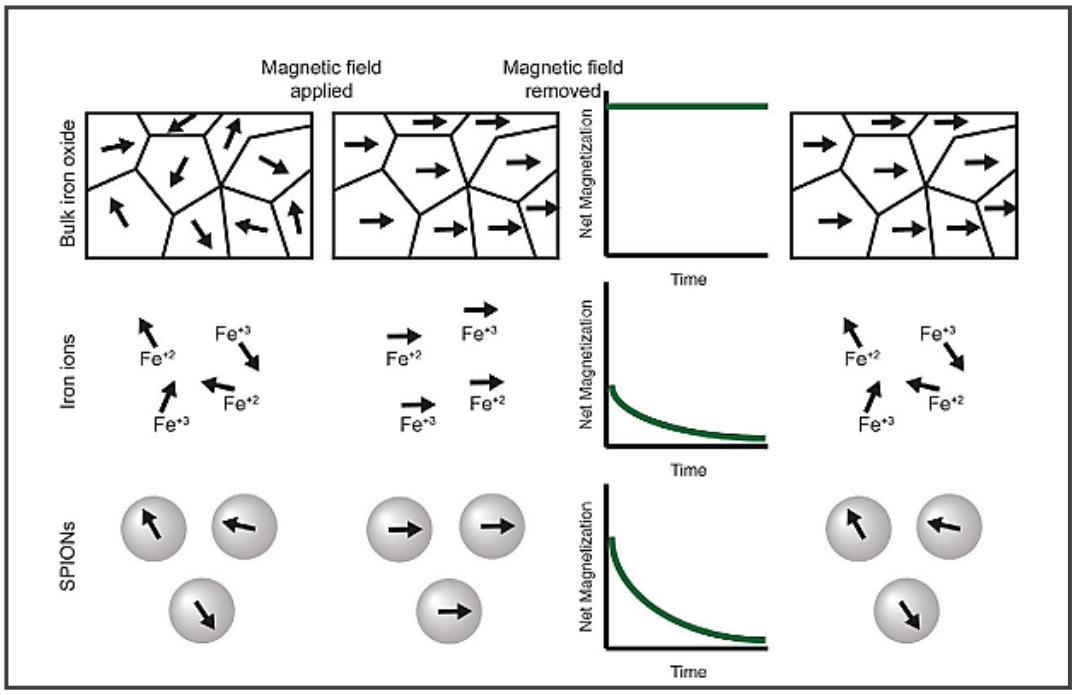

Figure 2.4. Effects of an external magnetic field on SPIONs (at the bottom), Fe ions (at the middle), and bulk magnetite (at the top). All magnetic moments are randomly aligned before the magnetic field is applied. The moments are aligned along the magnetic field's z-axis when an external magnetic field is applied. SPIONs have an initial net magnetization higher than Fe ions but lower than bulk magnetite. While the magnetic moments of both Fe ions and SPIONs gradually relax to equilibrium once the magnetic field is removed, the moments of bulk magnetite stay fixed along the z-axis [5]

Co-precipitation, thermal decomposition, solvothermal, and sol-gel are some of the synthesis methods to produce SPION. Compared to other approaches, each has its benefits and drawbacks. Although SPIONs offer many benefits, they also have drawbacks such aggregation, instability/easy oxidation, and biocompatibility. When it came to size reduction, those problems became more noticeable [39]. To avoid negative features/problems, magnetic nanoparticles require functional groups, coatings, and other methods.

Combination of especially two properties, magnetism and biocompatibility, became an advantage for the case of magnetic bioactive glasses. Aside from biocompatibility and magnetization, magnetic bioactive glasses could also be beneficial to enhance colloidal stability of the particles. In addition, it was demonstrated that the magnetization of magnetic bioactive glasses and the magnetic phase content had nearly linear relationship. As a result, as the magnetic phase in the glass composition increased, magnetic behavior would also improve [40].

Melt-quenching has been one of the asic procedures for producing magnetic bioactive glasses. Colloidal systems, on the other hand, have been frequently favored due to their numerous benefits. The findings have been continuously broadened in several papers.

Depending on the bioactive glass system design and necessary magnetization levels, the magnetic phases and their amounts could be alternated. According to Wu et al. [14], magnetic mesoporous bioactive glasses may be made by adding Fe^{+3} and Fe^{+2} ions. Fe_3O_4 components are produced in the magnetic mesoporous bioactive glass, giving the system a magnetic characteristic. They also showed continuous ion release with a varied loading range.

Shankhawar et al. [41] also showed that $41CaO–44SiO_2–4P_2O_5–8Fe_2O_3–3Na_2O$ bioactive glasses had both magnetic (magnetite and hematite) and bone minerals following heat treatments. They also showed the interplay of glassy matrix and crystalline iron oxide phases and variations in magnetic property for each sample. Making composite structure was one technique to improve the properties of bioactive glasses and their applications.

One strategy to improve the characteristics of bioactive glasses and their application regions was to produce them as composites. In Li et al. [19] observed behavioral improvement in the produced glasses. According to study Jalekshmi et al. [42], iron oxide chitosan-gelatin-bioactive glass composites were created with adequate magnetization and acceptable biocompatibility for drug delivery applications.

Magnetic phase integration with bioactive glass was found to modify bioactivity in various investigations., according to Hameed et al. [43], the rate of ferrimagnetic glass-ceramics apatite production would vary depending on the type of metal oxide added to the system. In short, increase in bioactivity may result in enhanced biological response, cell attachment and proliferation. As a result, magnetic phase served to improve the performance and broaden the use of these glassess. Zhu et al. [44] demonstrated that magnetic mesoporous bioactive glass composite scaffolds could restore critical-sized bone lesions and release certain medicines.

Wang et al. [40]. claim that superparamagnetic iron oxide nanoparticles may be used to create macro and mesoporous structures for drug storage and release. Furthermore, as compared to non-magnetic samples, bone regeneration ability is significantly increased. One of the simple ideas called core-shell structure was used to create magnetic bioactive glass particles in smaller sizes. The magnetic bioactive glasscore-shell structure was created using the sol-gel method. In summary, the core-shell structure is one of the methods to produce magnetic bioactive glass particles. In addition, Kesse et al. fabricated magnetic phases using co-precipitation techniques, and bioactive core-shells were produced using the sol-gel approach [39]. However, while magnetic nanoparticle cores covered with bioactive glass layer did not completely loose their magnetic behavior, the magnetization value decreased following the creation of a shell layer onto the core.

Appropriate biological tests are performed to examine the cytocompatibility and potential biological effects of magnetic bioactive glasses. As a result, the as synthesized magnetic bioactive glass samples showed no cytotoxicity when tested using the NHFB cell line in MTT experiments. After drug loading, significant inhibitory effects on cancer cell viability were detected [40]. In addition, Kesse et al.'s study demonstrated the interaction of human mesenchymal stem cells with magnetic bioactive glasses, and their findings were promising [39].

Finally, long-term in vivo investigations would give more precise information concerning the potential of magnetic bioactive glasses. The performance of magnetic

bioactive glass scaffolds that host bone integration ability was reviewed. Wang et al. [45] reported magnetic bioactive glass scaffolds to have host bone integration ability.

In this thesis, we fabricated two different types of magnetic bioactive glass particles. We characterized their magnetization, bioactivity and cytocompatibility in the presence and absence of external static magnetic.

CHAPTER 3

MATERIALS METHODS

3.1 Materials

$FeCl_2.4H_2O$ (Iron (II) chloride tetrahydrate), $FeCl_3.6H_2O$ (Iron (III) chloride hexahydrate), HCl (36%), ammonia solution (NH_3, 25%), and sodium sulfate (Na_2SO_4) were purchased from Merck. NaOH (≥97.0%), Tetraethyl orthosilicate (TEOS, 99%), triethyl phosphate (TEP, 99.8%), calcium nitrate tetrahydrate ($Ca(NO_3)_2.4H_2O$, CaN, 99%), sodium chloride (NaCl), sodium hydrogen carbonate ($NaHCO_3$), potassium chloride (KCl), di-potassium hydrogen phosphate trihydrate ($K_2HPO_4.3H_2O$), magnesium chloride hexahydrate ($MgCl_2.6H_2O$), calcium chloride ($CaCl_2$), tris-hydroxymethyl aminomethane ($(HOCH_2)_3CNH_2$), and Tris were purchased from Sigma Aldrich. All chemicals were used without any purification.

3.2 SPION Synthesis

Co-precipitation method was used to synthesize iron oxide (Fe_3O_4) nanoparticles. Briefly, $FeCl_2.4H_2O$ and $FeCl_3.6H_2O$ were mixed at 1:2 molar ratio in 0.8M HCl solution to improve the solubility of the iron salts. 1.5M NaOH (freshly prepared basic solution) was injected into the prepared salt solution at 80°C under N_2 environment to control oxidation. The reaction was ended in 25 min after obtaining a black-colored precipitate. SPIONs were rinsed three times with distilled water and ethanol to remove unreacted compounds. Then, particles were dried under a vacuum environment to prevent oxidation. Figure 3.1 illustrates the fabrication method for SPIONs production.

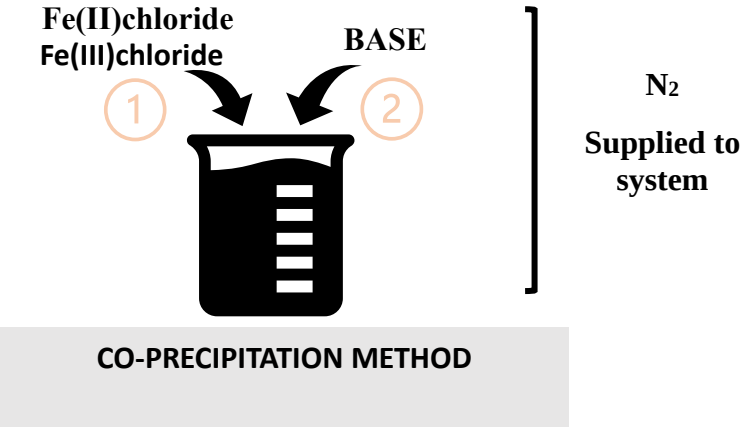

Figure 3.1. Fabrication schematic for SPIONs

3.3 SPION Embedded Bioactive Glass Synthesis

For the synthesis of SEBG nanoparticles, initially SPIONs were dispersed homogenously using an ultrasonic bath. First, 0.05g SPIONs were added to an alkaline solution (pH 11) with a water to ethanol ratio of 0.66 and dispersed for 60 min. Simultaneously, a second solution was prepared using 25 mL ethanol, 2.25 mL TEOS, and 0.23 mL TEP. After SPIONs were dispersed in the first solution, the second solution was immediately added into the first one to start nucleation of the bioactive glass nanoparticles on SPIONs. After one hour of mixing, CaN was added as Ca precursor to the mixture and mixed for another hour to promote growth of bioactive glass nanoparticles. At the end of one hour, particles were collected, rinsed three times with distilled water and ethanol. Then, particles were dried at 24h at 60°C. Following the drying step, calcination was applied at 700°C for 2h and Figure 3.2 indicates the SPION embedded glass synthesis. Additionally, Figure 3.4a indicated the SPION embedded bioactive glass design desired after the synthesis.

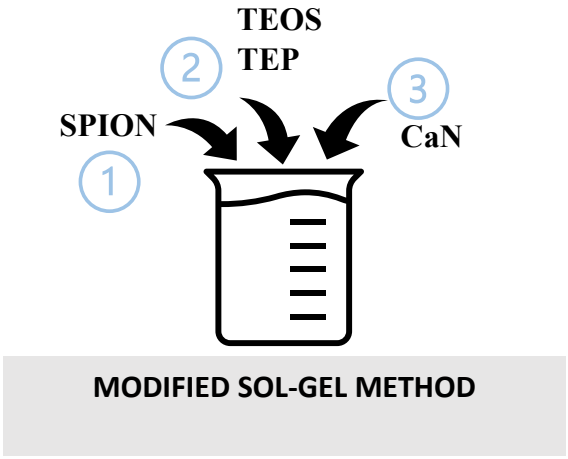

Figure 3.2. Fabrication schematic for SEBG nanoparticles

3.4 Bioactive Glass Synthesis

Before starting to the synthesis two solutions were prepared. The first solution was the basic/alkaline solution which is prepared using a 0.66 volume ratio of DW/Ethanol under 1.4M ammonia content. Ethanol, TEOS and TEP were used to prepare the second solution (TEOS/Ethanol volume ratio ~ 0.09). The second solution was then added to the first solution immediately to initiate the silica nucleation. CaN was introduced to the system after one hour of stirring, and mixing continued for another hour. Prior to drying, the particles were centrifuged and rinsed three times with water and ethanol to get rid of unreacted compounds from the system. Furthermore, the freeze-drying procedure was applied to eliminate the possible agglomeration of the particles. Finally, calcination was applied as a final step for 2h at 700°C to eliminate nitrates from the glass system.

3.5 SPION Deposited Bioactive Glass Synthesis

For the synthesis of SPION deposited bioactive glass nanoparticles, bioactive glass nanoparticles were produced. Then, similar to SPIONs production, SPION deposition was applied, and Figure 3.3 includes detailed illustration. Preprepared bioactive glass nanoparticles were used, and they were dispersed in distilled water at 0.1g/mL concentration using an ultrasonic bath. After 10 min of dispersion of bioactive glass nanoparticles, the ferric chloride solution ($FeCl_2.4H_2O$: $FeCl_3.6H_2O$, 1:2) was introduced to the system at 80°C. The pH of the solution was raised to around 11 by incorporation of ammonia to initiate SPIONs nucleation under N_2 atmosphere. The reaction was completed in 25 min after obtaining a black-colored precipitate. SDBG nanoparticles were collected and rinsed three times with distilled water and ethanol to remove unreacted components. As a last step, drying process was performed under vacuum for 24h to prevent possible oxidation of SPIONs. Figure 3.4b indicated the SPION deposited bioactive glass design desired after the synthesis.

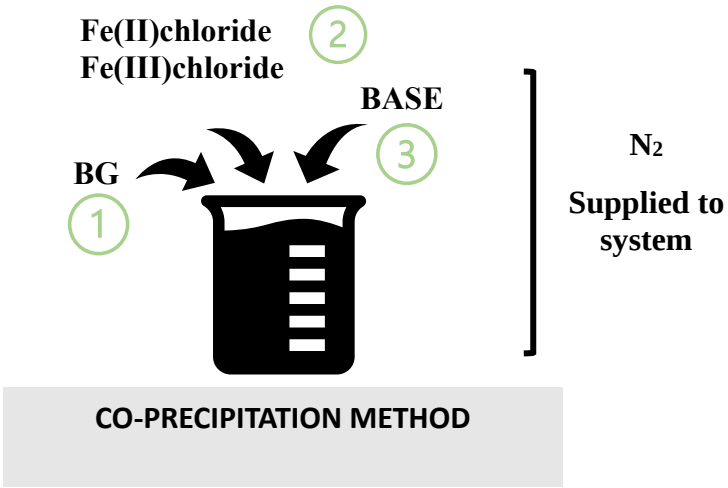

Figure 3.3. Fabrication schematic for SDBG nanoparticles

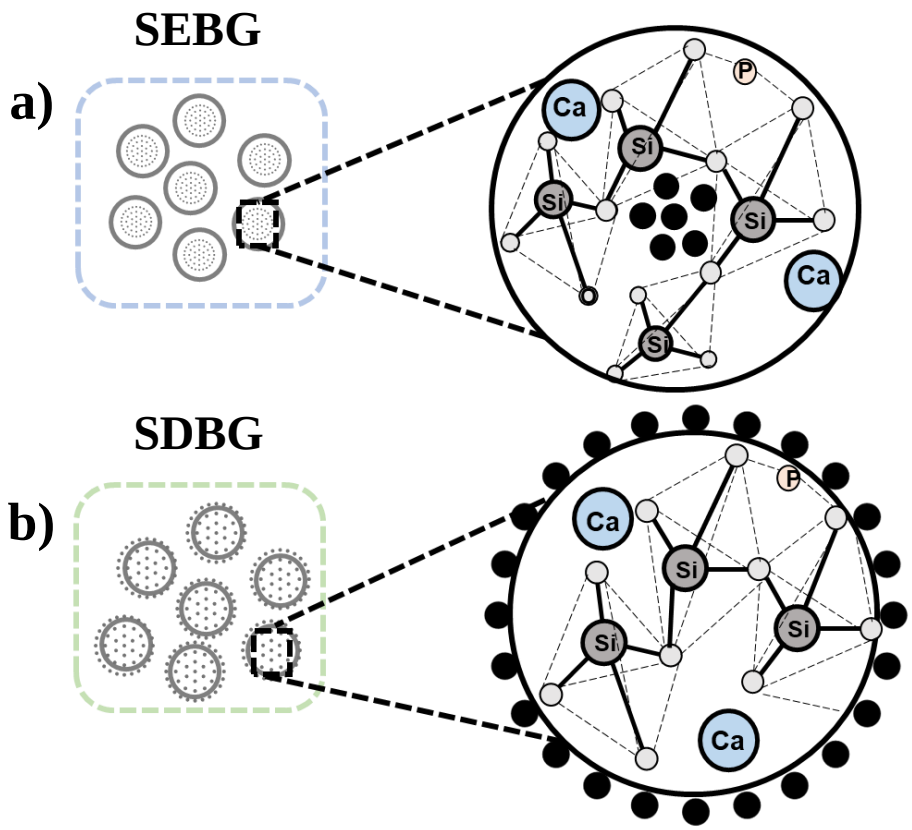

Figure 3.4. Schematic of a) SPION embedded bioactive glass nanoparticles, and b) SPION deposited bioactive glass nanoparticles

CHAPTER 4

CHARACTERIZATION TECHNIQUES

4.1 Scanning Electron Microscopy (SEM)

The FESEM FEI NOVA NANO 430 model was used to examine each nanoparticle morphology. Therefore, glass nanoparticles virtualize with high magnification and resolution. For the SEM investigation, all the synthesized nanoparticles were coated with gold for 3 min after particles being placed on the carbon tape.

4.2 Energy Dispersive Spectroscopy (EDS)

To confirmelemental compotions of each glass nanoparticles. Elemental composition (identifying and quantifying) was investigated at submicron resolution using a commonly installed energy dispersive X-ray spectroscopy (EDS) attachment. Therfore, EDS gave an elemenatal spectrum to compare the elemental weight percentages in glass nanoparticles.

4.3 Transmission Electron Microscopy (TEM)

The nanoparticles were prepared on grids after being diluted with ethanol. The solution was then dried on carbon-coated Cu TEM grids. The Jeol 2100F 200kV RTEM and FEI 120kV CTEM were used to take TEM images at various

magnifications using a 200kV accelerating voltage. TEM analysis was carried out by an electron beam to visualize nanoparticles with higher resolution. TEM analysis one of the common methods directly used to measure particle size, size distribution and morphology.

4.4 X-Ray Diffraction (XRD)

XRD utilized to determine crystalline and amorphous phases of the synthesized nanoparticles. XRD analyses were conducted with a Rigaku X-ray Diffractometer model instrument at 10-70° diffraction angles at 2°/min scanning speed using monochromatic Cu Kα radiation (40 kV, 30 mA). Diffraction patterns were collected for each nanoparticle.

4.5 Vibrating-Sample Magnetometer (VSM)

The magnetization characteristics of the nanoparticles were measured at room temperature with a magnetic field ranging from -1 to 1 Tesla (T) using a vibrating sample magnetometer (Cryogenic Limited PPMS). For the measurement, a 300 mg sample was employed. By the help of VSM analysis M-H curve could be obtained and saturation magnetization values could be determined for each nanoparticle. Besides, basic magnetic properties could be obtained with the hysteresis loops such as superparamagnetism.

4.6 Fourier Transformed Infrared Spectroscopy (FTIR)

The molecular bonding characteristics of the nanoparticles were determined using a Perkin Elmer 400 spectrometer and the KBr pellet technique in the mid-infrared (MIR) region of 4000-400 cm^{-1}. Depending on the spectrum, specific/characteristic molecular groups could be determined. Briefly, absorption bands showed the materials components for each sample.

4.7 Thermogravimetric Analysis (TA)

Thermal analysis of nanoparticles was conducted using TA Instruments SDT 650 Simultane TGA from 25°C to 1000°C at a heating rate of 10°C/min in N_2 environment to investigate thermal behavior of each sample. Thermal analysis provided information about materials by the mass change as a function of temperature in a certain atmosphere. Therefore, chemical transformations, sublimination, absorption, adsorption dehydration and decomposition could be observed by TGA curves.

4.8 Cell Culture

Human osteoblast cells (hFOB, ATCC CRL-11372) were cultured at 37°C (% CO_2) in Dulbecco's Modified Eagle's Medium containing 10% fetal bovine serum (FBS, Biological Industries, 04-001-1A), 1% penicillin-streptomycin (Biological Industries, 03-031-1B), and 1% L-glutamine (Biological Industries, 03-020-1B) (DMEM, Sigma Aldrich D6429).

4.9 MTT Assay

For MTT assays, two types of media were prepared as direct contact and indirect contact (extract). Three MTT designs were created in presence and absence of magnetic field. Therefore, by the help of those designs the effect of magnetic field on cells could be evaluated. Results were given as direct contact samples both in presence and absence of magnetic field.

The hFOB's metabolic activity was measured using an MTT assay. All samples were sterilized with 70% (v/o) ethanol, 1xPBS, and UV-light for 60 min before the MTT assay. After completing the sterilization steps, cells were seeded on 96-well plates with a density of 10,000 cells per well. Afterwards, seeded cells were incubated at 37°C for 24h in a humidified environment (5% CO_2 at 37°C). Following that, the cells were cultured in DMEM with a certain nanoparticle concentration for each sample (1mg/mL) for up to 7 days (direct contact). On the first, third, fifth and seventh days, after the aspiration, each well was washed with 1xPBS. Then, 125 mL of 3-(4,5-dimethyl-2-thiazolyl)-2,5-diphenyl-2H-tetrazolium bromide (MTT) was added to each well, and the mixture was incubated for 4h to create formazan crystals. Additionally, the same procedure was applied again by using magnetic plated to evaluate magnetic field effect. Using a Multiskan GO spectrophotometer from Thermo Scientific, the optical density was measured at 570 nm. Experiments were performed in each sample for the three times. One-way analysis (ANOVA) and Tukey's post hoc test were used by SPSS software to analyze the data, with $*p<0.05$ significance.

Extract samples were prepared in DMEM with a particle concentration of 1 mg/mL and incubated at 37°C for 72h. After extract samples were prepared, cells were seeded on 96-well plates with a density of 10,000 cells per well and then incubated for 24h in humidified environment (5% CO_2 at 37°C). Each well was washed twice with 1xPBS after the medium was aspirated on the first, third, fifth and seventh days. After that, each well was filled with 125 mL of 3-(4,5-dimethyl-2-thiazolyl)-2,5-diphenyl-2H-tetrazolium bromide (MTT), which was incubated for 4 hours to

develop formazan crystals. The optical density at 570 nm was measured using a Thermo Scientific Multiskan GO spectrophotometer. The experiment was done three times with three repeats in each run. The data were examined in SPSS software using one-way analysis of variance (ANOVA) with Tukey's post hoc test, with *$p<0.05$ indicating significance.

4.10 Magnetic field Simulations

COMSOL Multiphysics version 5.5 was utilized to calculate magnetic field strength for each well. A 3D model was designed with 24 permanent magnets and those plates were placed under wells. Magnets were placed in plate as a 4x6 grid with 18 mm center to center distance, which left one empty along both directions.

4.11 Simulated Body Fluid (SBF) Preparation

The in vitro bioactivity of the samples was evaluated by the Simulated Body Fluid (SBF) immersion test, as described by Kokubo et al.[26]. The compound list and amount of the reagents with the addition order was illustrated in table 4.1.

Table 4.1. Prepared Simulated Body Fluid (SBF) solution reagents and amounts were given with addition order [27]

Order of addition to the vessel	Reagent	Amount	Purity (%)	MW
1	NaCl	8.035 g	99.5	58.4430
2	$NaHCO_3$	0.355 g	99.5	84.0068
3	KCl	0.225 g	99.5	74.5515
4	$K_2HPO_4.3H_2O$	0.231 g	99.0	228.2220
5	$MgCl_2.6H_2O$	0.311 g	98.0	203.3034
6	1.0 M–HCl	39 ml	–	–
7	$CaCl_2$	0.292 g	95.0	110.9848
8	Na_2SO_4	0.072 g	99.0	142.0428
9	Tris	6.118 g	99.0	121.1356
10	1.0 M–HCl	0–5 ml	–	–

To prevent nucleation, SBF solution was prepared in a plastic container. Then, each reagent was weighed for 1000 mL SBF preparation. Then, preparation was started with the 700 mL of distilled water heated up to 36.5±1.5°C. Ingredients was added one by one with an order (given in table a list) once at a time.

As noted, each reagent was added to until dissolving completed totally without precipitation. During the progress temperature control was also necessary to prevent precipitation. As a last step, tris was added to the solution slowly and carefully.

During that step the pH was below 7.45 while keeping the temperature at 36.5°C, the pH needed to raise slowly. Without precipitation, all the weighted Tris needed to dissolve in a pH 7.45 environment. If necessary 1M-HCl was added dropwise to the solution in range (0-5 mL), to maintain the pH of the solution in the safe range. After the entire amount of Tris had dissolved, the temperature was set at 36.5°C. Then, pH was adjusted as given a value of 7.40. When the solution was completed with distilled water to its final volume, the preparation process was complete. Afterwards, the prepared solution was carefully cooled to 20°C without any precipitation.

For seven days at 37°C, samples were soaked in SBF solution with a particle concentration of 1 mg/mL. The samples were then dried at 60°C after being rinsed in distilled water.

CHAPTER 5

RESULTS AND DISCUSSION

Scanning electron microscopy (SEM) results were shown in Figure 5.1. SEM images demonstrated that magnetic bioactive glass nanoparticles were successfully synthesized with both fabrication systems. Moreover, SPIONs were effectively produced with co-precipitation technique, and they had irregular morphology as expected. Similarly several studies showed that co-precipitation method provides irregular morphology [20,28,29].

Additional to that, spherical morphology was not observed for SPION embedded bioactive glass nanoparticles. In short, since fabrication process relied on the nucleation of silica nanoparticles on SPIONs by modified sol-gel (stöber) technique, the morphology of SEBG nanoparticle has been inevitable. Since BG nanoparticles were already produced by stöber method SDBG had spherical morphology. SPIONs created a thick layer on the BG nanoparticles where iron salts nucleated and grew as desired.

In short, while the smoother round shape was obtained for SDBG particles. Due to the SPIONs presence within the nanoparticles, SEBG samples did not have spherical morphology. Namely, the irregular morphology of SPIONs led to spheroidal-like fused morphology.

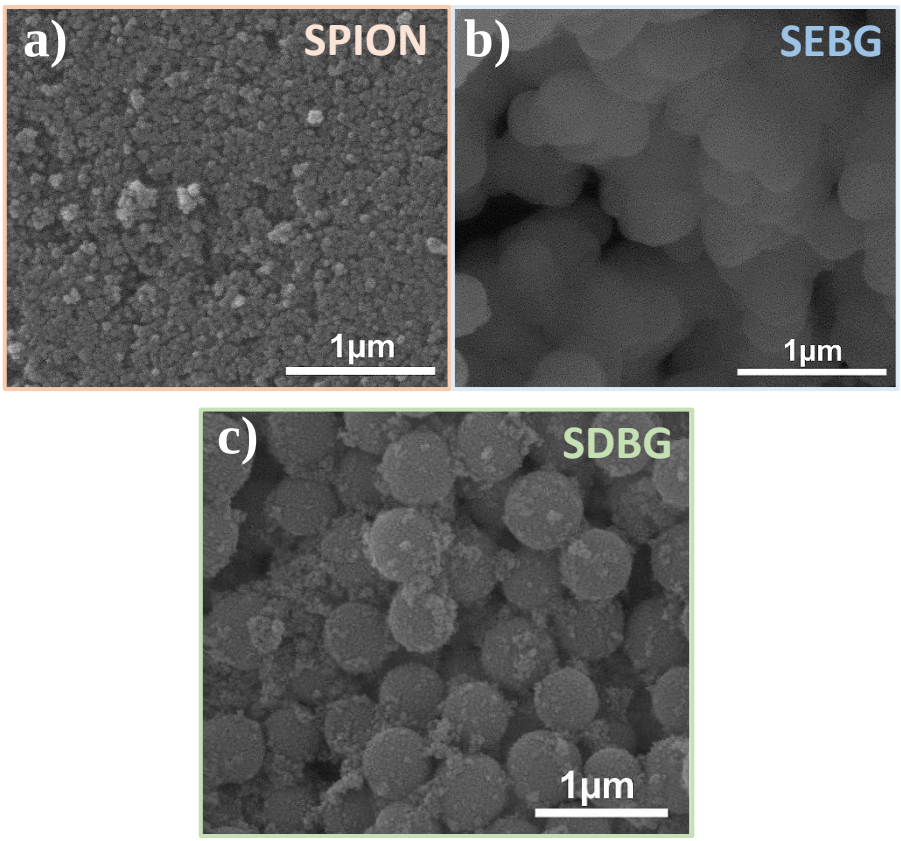

Figure 5.1. SEM images of a) SPIONs, b) SEBG and c) SDBG nanoparticles (scale bars are 1µm)

Transmission Electron Microscopy (TEM) analysis was employed to verify the SEM findings and closely examine the morphology, structure, and size of synthesized nanoparticles for each system. In addition, diffraction pattern was obtained from SPIONs synthesized by co-precipitation to identify and demonstrate sample.

Briefly, diffraction pattern was used to prove that the crystal phase formed obtained as Fe_3O_4 [30,31]. Similar to SEM results, spherical morphology was observed of both magnetic bioactive glass systems and irregular morphology for the SPIONs was observed in Figure 5.2 TEM images.

ImageJ software was used to process the size measurements for each nanoparticle systems. measurements were achieved by measuring over two hundred particles. In particular, SEBG nanoparticles were measured as closest to the diameter for nanoparticles. By using a log-normal function to fit histogram, the average diameter determined for both SEBG and SDBG were 180 ± 9 nm and 420 ± 10 nm. Since production relied on the classical nucleation theory, SPIONs with only a decent amount of size polydispersity have been produced [29,32]. This was apparently due to a process overlap between the nucleation and growth phases during the addition of basic solution [33,34]. The difference between average particle sizes for magnetic bioactive glass nanoparticles could be explained by the nucleation and growth rate. During SDBG nanoparticle synthesis, silica particles nucleated homogeneously, and the growth mechanism worked immediately. Though, for SEBG nanoparticles, bioactive glass grew on SPION clusters in an aqueous solution. The effectiveness of SPION dispersion inside the solution determined the surface contact between the glass phase surrounding the particles, which in turn limited the particle size generated using this approach. It really was probable that efficient SPION dispersion within the aqueous solution enabled SPION clusters to be positioned close together, which upon particle growth resulted in smaller SEBG nanoparticles. It is possible that SEBG nanoparticles started interacting with one another while particle development was still occurring, which would account for the resulting fused-like particle shape. Additionally, TEM images also demonstrated that homogeny was olso observed for each sample. Consequently, all fabricaiton systems worked sucessfully.

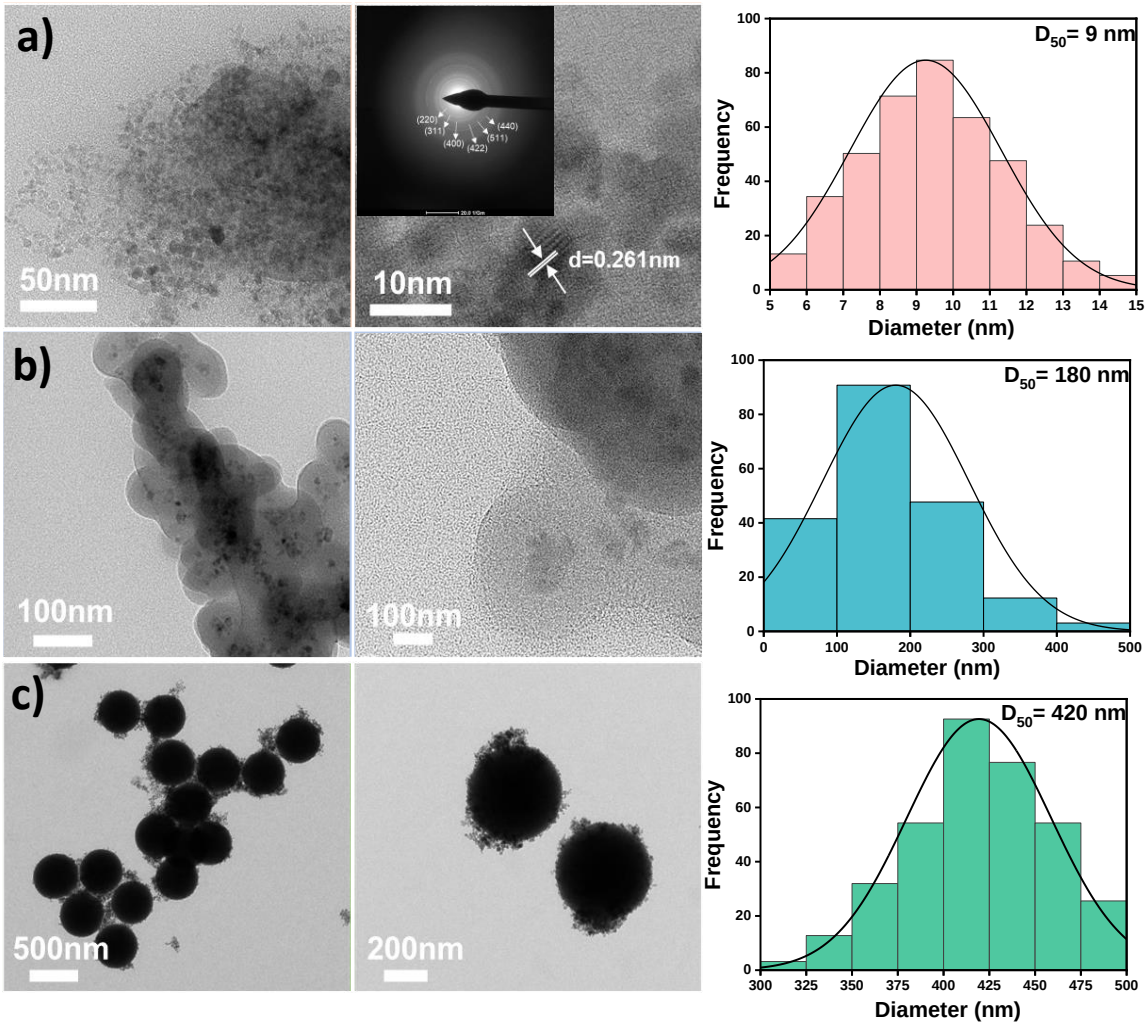

Figure 5.2. TEM images and the particle size distribution for a) SPION, b) SEBG and c) SDBG nanoparticles

X-ray diffraction (XRD) examination was required for more detailed data on the structure of synthesized particles. As shown in diffraction patterns obtained from TEM images, again expected crystal peaks came from magnetic phase came from SPIONs. Besides, an amorphous silica hump was obtained in SEBG and SDBG (seen in Figure 5.3). Amorphous silica hump was more prominent for SEBG with respect to SDBG. The reason for that could be briefly explained by the bioactive glass formation on the SEBG nanoparticles. However, particles had a thick SPION layer outside of the BG nanoparticles for the SDBG nanoparticles. Therefore, silica hump was less prominent. Moreover, magnetic phase peaks planes were shown as hkl values (220), (311), (400), (422), (511), (440). Additionally, XRD spectra was given in Figure 5.3 and the crystal phase peaks belonged to magnetic phase (JCPDS 19-0629) and a 20–25° amorphous silica hump (JCPDS 82–1574). Consequently, XRD data showed that production techniques worked effectively when producing nanoparticles for both systems and silica hump was more significant for SEBG nanoparticles [35,36].

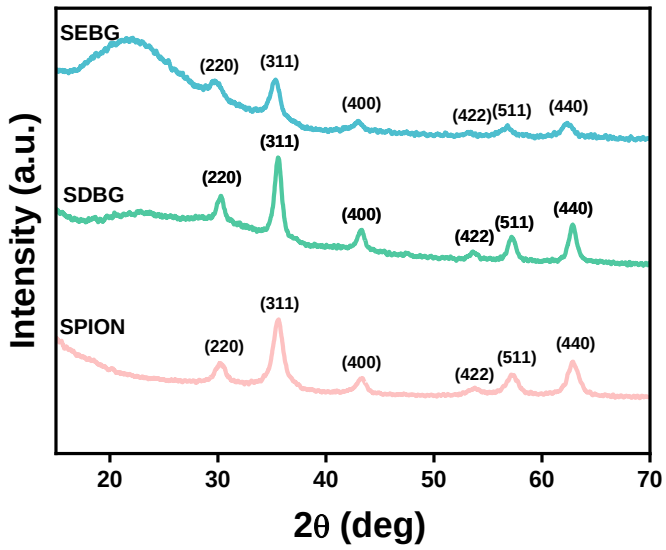

Figure 5.3. XRD spectra of SPION, SEBG and SDBG nanoparticles

Magnetic properties of the nanoparticles are measured by using a vibrating-sample magnetometer (VSM) at room temperature to obtain hysteresis curves for each sample. Saturation magnetization values (Ms) were obtained from Figure 5.4 with M-H curves for SEBG and SDBG nanoparticles. It was clear that Ms value was decreasing 4 emu/g for SEBG and 9 emu/g for SDBG. Magnetization characteristics demonstrate that both nanoparticles showed zero coercivity and zero remanence [15,37–39]. Primary results were indicating that the particles could be candidate materials for biomedical applications as they were targetable with zero coercivity.

The decrease in magnetization was related to the thick bioactive glass layer created around the SPIONs of the synthesized magnetic bioactive glasses therefore as the shell thickness increases magnetization values decreases. Particle size increase effect decreased magnetization value for both particles. Similar to the litearure, the magnetization decrase could direcly related to the created silica layer and heat treament conditions[17,36].

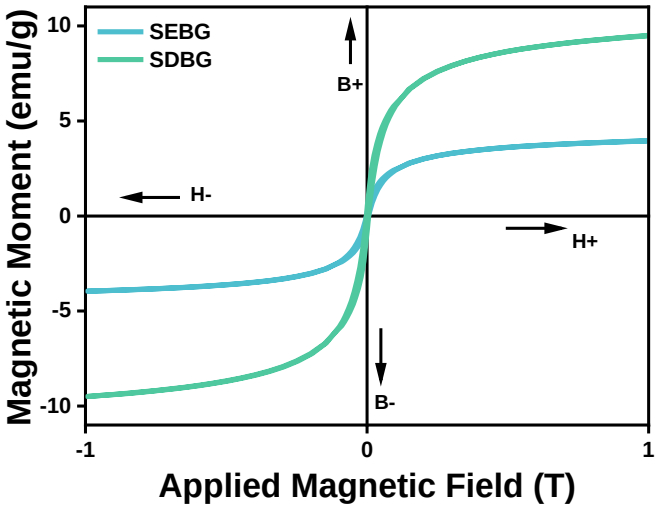

Figure 5.4. M-H hysteresis curves of SEBG and SDBG nanoparticles

In Figure 5.5, FTIR results showed all characteristic bands exist in each system, respectively. SPION originated from Fe–O stretching vibrations (570cm^{-1}) of the iron oxide cores. The weak band and the broadbands were attributed to the adsorbed water and surface hydroxyl groups (–OH). The bands were shown in Figure 5.5 as 1632 and 3432cm^{-1}.

Since silica is the major component of the BG nanoparticles, Si-O-Si bands were existing at 813cm^{-1} and 465cm^{-1} in the glass systems. Besides, asymmetric P-O bands (1097cm^{-1}) were present due to phosphate component of the bioactive glass in both SEBG and SDBG nanoparticles. Additionally, the extra -OH group (3434cm^{-1}) was present in the magnetic bioactive glass nanoparticles represent water absorption [40–42].

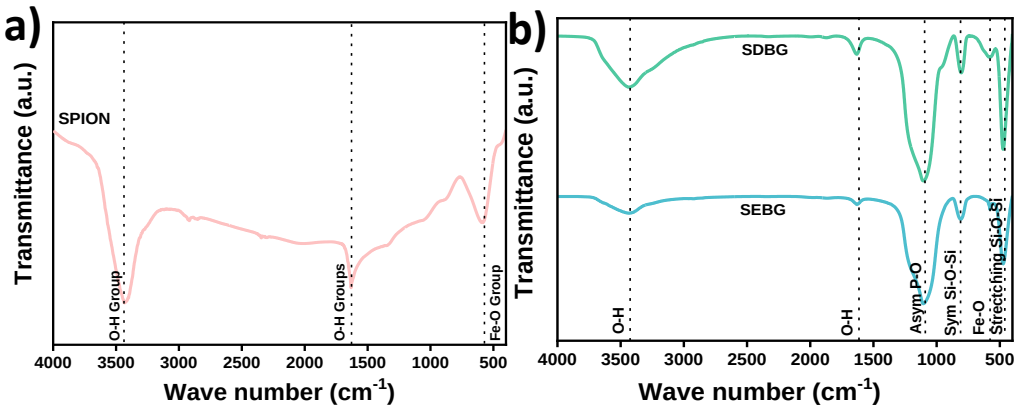

Figure 5.5. FTIR spectra of a) SPIONs, b) SEBG and SDBG nanoparticles

Figure 5.6 showed the TGA curve for dried bioactive glass sample to evaluate the thermal behavior of the samples as a function of increasing temperature and weight loss is observed in three main steps.

Total weight loss was evaluated as 14% for SPION embedded bioactive glass nanoparticles. The first step was between 25ºC and 300ºC and between that range water and alcohol was removed from the glass system.

During the second step which is between 450ºC and 600ºC, nitrates detachment is observed. Besides, after 600ºC weight loss was seen constant which indicates the stabilization of the glass.

Last step was related to the beginning of the crystallization which was defined as 800ºC for the sample. Consequently, decided heat treatment temperature used in synthesis (700ºC) which proofed that heat treatment temperature was enough to promote complete elimination of nitrates (without crystallization), as the crystallization was only observed at temperatures higher than 800ºC [40,43–45].

Additionally, since SDBG samples were prepared by BG particles (heat treatment applied), TGA results for SDBG particles showed the almost the same behavior with SPIONs and 7% total weight loss [46].

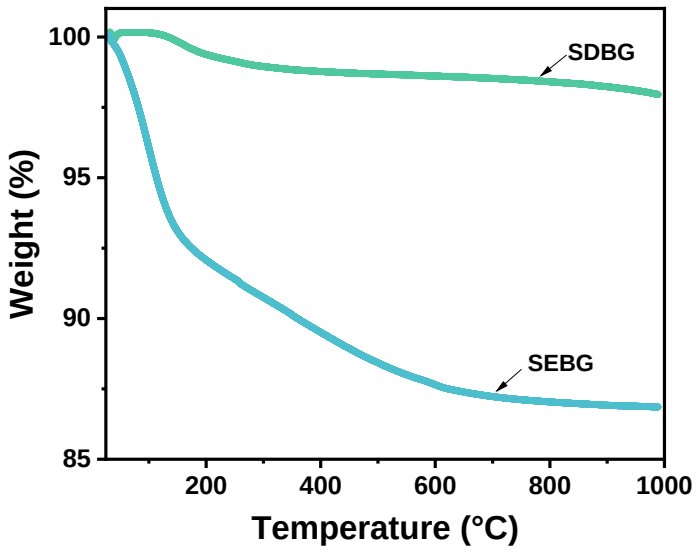

Figure 5.6. Thermogravimetric analysis curve for SEBG and SDBG nanoparticles

By soaking the sample in simulating body fluid (SBF), a salt solution resembling the inorganic component of human plasma, and monitoring the sample mineralization process, the bioactivity of both synthesized magnetic bioactive glass nanoparticles were addressed (hydroxyapatite formation) [2,47].

After 7 days of SBF soaking for two magnetic bioactive glass nanoparticles, on the surface of the particles, a heterogeneous development of crystals could be obtained. X-ray diffraction and FTIR spectra have been used to determine HCA formation on the glass surfaces.

In Figure 5.7c, XRD pattern revealed that are typical of hydroxyapatite (JCPDS 09-0432) [48]. Besides, additional to apatite phase, peaks coming from the magnetic phase (SPION) was indicated by XRD results. Basically, all essential hkl planes were demonstrated according to the magnetic phase existence of peaks [49].

Since the same HCA layer formation observed for the two particles and all related characterizations were given in Figure 5.7. SEM images were shown in Figure 5.7a for both nanoparticles. SDBG nanoparticles had higher particle size showed slower crystallization compared to the SEBG samples. Briefly, the particle size was one of the determining factors for the HCA layer formation rates. Similarly, according to several studies, rate of HCA layer formation was related to the rate of interaction of the bioactive glass surfaces [9,50–53]. In short, the particle size of bioactive glasses had a direct impact on the reaction rate during SBF interaction. As a result, as particle size decreased, ion exchange and crystallization steps were completed more quickly [54,55]. Besides, particle surfaces have been gaining importance because it was promoting faster crystallization on the glass surface when core was SPION compared to the SPION was deposited the glass sample. Furthermore, when SPION was deposited on the glass surface (SDBG), slower crystallization behavior was observed because the BG surface could not contact directly. As a result, all the steps were happened more rapidly for SEBG samples with respect to the SDBG samples.

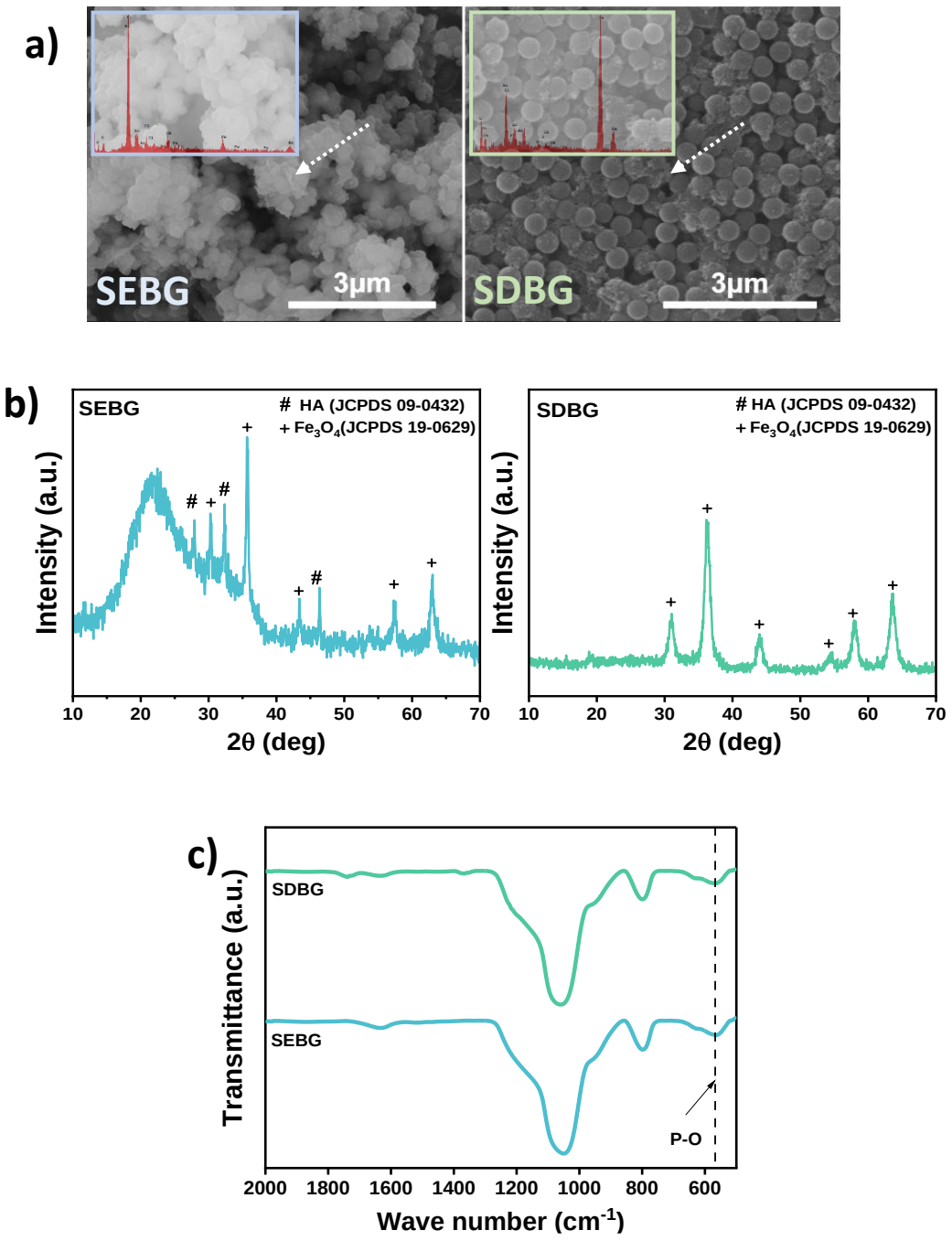

Figure 5.7. a) SEM images, b) XRD and c) FTIR spectra of SEBG and SDBG nanoparticles after being soaked in the simulated body fluid for 7 days

Figure 5.8 indicates the magnetic plate used in MTT assays to crate static magnetic field and magnetic field strength for created by neodymium magnets in x and y direction. Here, the effect of the magnetic field created by the magnetic plate was expressed. Briefly, how the well plate system was set up and cells/particles were affected in these circumstances are simply summarized. It was proven that there is no magnetization in the region of wells where magnets do not exist. COMSOL program computed the magnetic field strength field in the x, y, and z planes as the highest strength exhibited in red and the lowest strength shown in blue. The 24 wells magnetic field conditions were equal for each well with a mean strength of 0.4T, and these values were achieved by spacing the magnets apart by leaving one empty well in between.

Figure 5.8. Schematics of the magnetic plate and placement of the neodymium magnet on the cell culture plate surface

Bone cells proliferated in vitro following treatment with bioactive glass samples. To observe the cytotoxic effects of the magnetic bioactive glass nanoparticles, MTT assay results were displayed for up to 7 days and results were shown in Figure 5.9. SDBG and SEBG demonstrated improved cell proliferation compared to other groups, particularly on days 3 and 7 [56]. Day 3 exhibited increase in the SDBG and SEBG samples compared to control group of 21% and 18%, respectively. The increase in direct contact samples about 20% and 10% in day 7 with respect to the control group for SDBG and SEBG samples. According to SEM and TEM pictures, the presence of SPIONs caused the SDBG nanoparticle surfaces to become rougher,

which may have boosted hFOB viability. Additionally, the increase in nanoparticle size for SEBG may have resulted in improved interactions with cells

Particularly under magnetic field, SDBG gave better cell responses after third day. According to the results obtained on day 3 and day 7, 15% increase was observed with respect to the control group for SDBG. Indirect contact MTT results showed that specially on day 7, SDBG and SEBG samples 10% and 19% respectively. Indirect contact results proofed the extract medium of SEBG gives better cell responses with respect to other groups [16,17,56,57]. The reason for that could be related to the easy therapeutic ion release [12] for SEBG with respect to the SDBG samples. Those results could be briefly associated with SBF interactions because SEBG indicated faster mineralization with respect to the SDBG samples. Thus, samples having higher mineralization rate could interact with bone cells faster and increase the number of cells.

According to studies, ionic dissolution products were demonstrated to play vital roles in bone metabolism processes, such as bone tissue formation, calcification, collagen creation, osteoblast proliferation and differentiation, and extracellular matrix mineralization [36]. Besides, it could also be related to the smaller particle size with respect to the SDBG nanoparticles which was relayed to the easy crystallization and faster dissolution due to higher surface areas. In addition, depending on the primary MTT assays SPION did not show any toxic effect on osteoblasts. This effect was more significant on direct and indirect contact samples. Although, working concentration was under toxic limit; under magnetic field SPION cell proliferation was shown to be reduced. This could be attributed to increased particle accumulation, presumably due to intense magnetization [58–61].

Overall, cell culture data showed that physical contact with the osteoblasts for the magnetic glass nanoparticles affected their viability rather than their dissolution products. Surface roughness was a significant feature that encouraged cellular viability. Cellular response may vary depending on the texture and roughness of the particle. Studies have shown that nanoparticle surface shape greatly affects cellular

functions in vitro [41]. For instance, cellular responsiveness may be enhanced by smaller surface features (50 nm) produced on silica nanoparticles as opposed to larger surface features. [38,42].

In this study, we suggested a method for creating magnetic bioactive glass nanoparticles by fusing SPION's superparamagnetic capabilities with the biocompatible and bioactive properties of glass nanoparticles driven by sol-gel. Regardless of whether SPIONs were deposited on the surface or incorporated into the bioactive glass nanoparticles, successful results were obtained both in the presence and absence of an external static magnetic field. Despite this, the results of the indirect contact experiment did not show any negative effects of any particle on osteoblasts. However, when SPIONs were applied to bioactive glass nanoparticles, magnetization and osteoblast viability increased. In actuality, both magnetic bioactive glass nanoparticles had minimum saturation magnetization values that were higher than those reported in comparable research in the literature [36]. This study's effective synthesis of biocompatible and targetable magnetic bioactive glass nanoparticles. The produced magnetic bioactive glass nanoparticles might make good candidate materials for a range of biomedical uses, including targeted treatments.

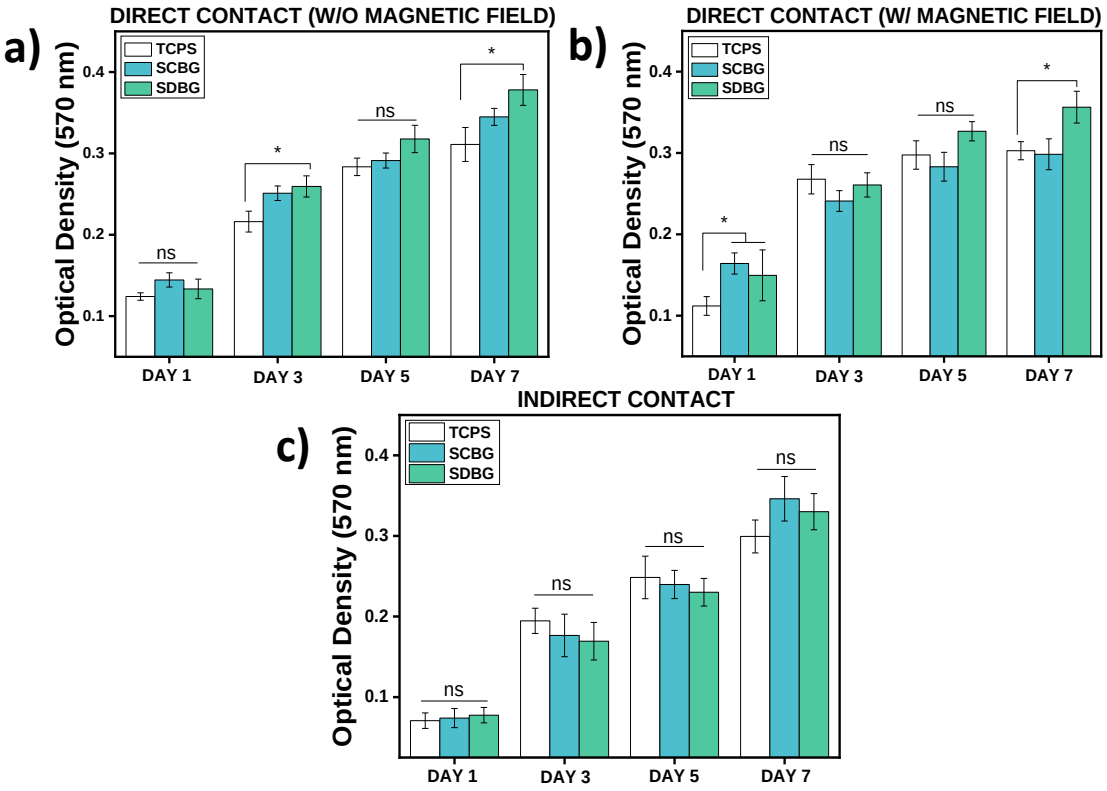

Figure 5.9. Osteoblast viability up to 7 days *in vitro* for direct contact a) absence and b) in the presence of magnetic field, and c) indirect contact experimental designs. Data are mean±SE, p*<0.05, ns: non-significant, particle concentrations are 0.1 g/L

CHAPTER 6

CONCLUSION

Due to their bioactivity and extensive customization potential, magnetic bioactive glasses and magnetic bioactive glass ceramics stand out among other magnetic materials as intriguing materials. The composition choice and processing procedures covered in this thesis proves that various characteristics of magnetic glasses could be improved. The true nature of certain additives must be better understood to develop suitable biomaterials for accurate biological applications.

In this study, superparamagnetic iron oxide nanoparticles were used to create magnetic bioactive nanoparticles created using a multi-step design process. A straightforward co-precipitation procedure was used to prepare the SPION and then SEBG nanoparticles were synthesized with sol-gel silica (a modified sol-gel/Stöber approach) onto the SPIONs. In addition, pre-synthesized BG nanoparticles were prepared to cover their surfaces with SPION again using co-precipitation to synthesize SDBG nanoparticles. SEM and TEM analysis confirmed successful synthesis of both magnetic bioactive glass nanoparticle. The size of nanoparticles for SPION, SEBG and SDBG were evaluated as 9 ± 0.5 nm, 180 ± 9 nm, 420 ± 10 nm respectively. Besides, magnetic bioactive glass nanoparticles expressed crystal peaks originating from the magnetic phase and amorphous silica humps. FTIR results showed characteristic bands for each system. Room temperature magnetization values for SEBG and SDBG particles were 4 and 9emu/g, respectively. The obtained spectral properties show that nanoparticles had zero coercivity and remanence.

Bioactivity was evaluated for the synthesized magnetic bioactive glasses nanoparticles by soaking in SBF for seven days and the results showed precipitation of hydroxyapatite on nanoparticle surfaces. Primary cellular responses were

evaluated by in vitro MTT assay and the results showed successful proliferation of bone cells after being treated with magnetic bioactive glass samples up to 7 days.

After briefly summarizing the results, it is necessary to discuss our objectives and results closely. Especially magnetization values obtained from two bioactive glass systems were higher than the ones obtained in literature which was around 2 emu/g [36,62]. In addition, the cell viability tests showed bone cells were viable up to 7 days of culture both in the presence and absence of external static magnetic field. Therefore, the synthesized nanoparticle could be used to target them to desired location in the body.

FUTURE WORK

In this work, several challenges related to magnetic bioactive glass were tackled, including convenient control of the synthesis parameters, maintaining the magnetization after nanoparticle synthesis, and cytotoxicity of the nanoparticles. However, there are still unexplored issues remain to be investigated in future studies.

Two of the main problems that needs to be addressed are low magnetization values and potential therapeutic effects. Magnetization value obtained in this thesis was 9 emu/g for SPION deposited bioactive glass nanoparticles. Although saturation magnetization values were higher than similar studies in the literature, future studies could be structured to improve the values of saturation magnetization to expand the application areas of magnetic bioactive glass nanoparticles. Improvements in magnetization value could be obtained by decreasing the particle size of the magnetic bioactive glass nanoparticles and increase in magnetic phase amount for each particle. The second avenue to be explored is improvement of the therapeutic effect of bioactive glass nanoparticles. Ion incorporation, i.e. strontium and silver, into the glass structure, would address this issue. By the ion incorporation, magnetic bioactive glass nanoparticles could have capability to show improved cellular response or antibacterial properties, and thus help alleviate critical healthcare issues. In addition, in vivo experiments can be designed to address efficacy of the particles in more realistic scenarios.

REFERENCES

1. Jones JR, Brauer DS, Hupa L, Greenspan DC. Bioglass and Bioactive Glasses and Their Impact on Healthcare. Int J Appl Glass Sci. 2016;7:423–34.

2. Yousefi A-M, Oudadesse H, Akbarzadeh R, Wers E, Lucas-Girot A. Physical and Tablebiological characteristics of nanohydroxyapatite and bioactive glasses used for bone tissue engineering. Nanotechnology Reviews. 2014;3.

3. Stephen ZR, Kievit FM, Zhang M. Magnetite nanoparticles for medical MR imaging. Mater Today. 2011;14:330–8.

4. Hench LL. The story of Bioglass®. J Mater Sci Mater Med. 2006;17:967–78.

5. Hench LL. Bioceramics. J Am Ceram Soc. 1998;81:1705–28.

6. Hench LL, Splinter RJ, Allen WC, Greenlee TK. Bonding mechanisms at the interface of ceramic prosthetic materials. J Biomed Mater Res. 1971;5:117–41.

7. Jones J, Baino F, Boccaccini AR. Special Issue: 50 Years of Bioactive Glasses: celebratory special issue in “Biomedical Glasses.” Biomed Glas. 2019;5:203–4.

8. Hench LL, Paschall HA. Direct chemical bond of bioactive glass-ceramic materials to bone and muscle. J Biomed Mater Res. 1973;7:25–42.

9. Kaur G, Pandey OP, Singh K, Homa D, Scott B, Pickrell G. A review of bioactive glasses: Their structure, properties, fabrication and apatite formation. J Biomed Mater Res A. 2014;102:254–74.

10. Ardeshirylajimi A, Farhadian S, Jamshidi Adegani F, Mirzaei S, Soufi Zomorrod M, Langroudi L, et al. Enhanced osteoconductivity of polyethersulphone nanofibres

loaded with bioactive glass nanoparticles in *in vitro* and *in vivo* models. Cell Prolif. 2015;48:455–64.

11. Cannillo V, Salvatori R, Bergamini S, Bellucci D, Bertoldi C. Bioactive Glasses in Periodontal Regeneration: Existing Strategies and Future Prospects—A Literature Review. Materials. Multidisciplinary Digital Publishing Institute; 2022;15:2194.

12. Chaichana W, Insee K, Chanachai S, Benjakul S, Aupaphong V, Naruphontjirakul P, et al. Physical/mechanical and antibacterial properties of orthodontic adhesives containing Sr-bioactive glass nanoparticles, calcium phosphate, and andrographolide. Sci Rep. 2022;12:6635.

13. Al-Harbi N, Mohammed H, Al-Hadeethi Y, Bakry AS, Umar A, Hussein MA, et al. Silica-Based Bioactive Glasses and Their Applications in Hard Tissue Regeneration: A Review. Pharmaceuticals. 2021;14:75.

14. Wallyn J, Anton N, Vandamme TF. Synthesis, Principles, and Properties of Magnetite Nanoparticles for In Vivo Imaging Applications—A Review. Pharmaceutics. Multidisciplinary Digital Publishing Institute; 2019;11:601.

15. Wu W, Wu Z, Yu T, Jiang C, Kim W-S. Recent progress on magnetic iron oxide nanoparticles: synthesis, surface functional strategies and biomedical applications. Sci Technol Adv Mater. 2015;16:023501.

16. Amini Z, Rudsary SS, Shahraeini SS, Dizaji BF, Goleij P, Bakhtiari A, et al. Magnetic bioactive glasses/Cisplatin loaded-chitosan (CS)-grafted- poly (ε-caprolactone) nanofibers against bone cancer treatment. Carbohydr Polym. 2021;258:117680.

17. Borges R, Mendonça-Ferreira L, Rettori C, Pereira ISO, Baino F, Marchi J. New sol-gel-derived magnetic bioactive glass-ceramics containing superparamagnetic hematite nanocrystals for hyperthermia application. Mater Sci Eng C. 2021;120:111692.

18. Yazdanpanah A, Moztarzadeh F. Synthesis and characterization of Barium–Iron containing magnetic bioactive glasses: The effect of magnetic component on structure and in vitro bioactivity. Colloids Surf B Biointerfaces. 2019;176:27–37.

19. Choi J, Cha J, Lee JK. Synthesis of various magnetite nanoparticles through simple phase transformation and their shape-dependent magnetic properties. RSC Adv. 2013;3:8365–71.

20. Mahmoudi M, Sant S, Wang B, Laurent S, Sen T. Superparamagnetic iron oxide nanoparticles (SPIONs): Development, surface modification and applications in chemotherapy. Adv Drug Deliv Rev. 2011;63:24–46.

21. Stephen ZR, Kievit FM, Zhang M. Magnetite nanoparticles for medical MR imaging. Mater Today. 2011;14:330–8.

22. Zhu Y, Wu C, Ramaswamy Y, Kockrick E, Simon P, Kaskel S, et al. Preparation, characterization and in vitro bioactivity of mesoporous bioactive glasses (MBGs) scaffolds for bone tissue engineering. Microporous Mesoporous Mater. 2008;112:494–503.

23. Kumar CSSR, Mohammad F. Magnetic nanomaterials for hyperthermia-based therapy and controlled drug delivery. Adv Drug Deliv Rev. 2011;63:789–808.

24. Tadić M, Kusigerski V, Marković D, Panjan M, Milošević I, Spasojević V. Highly crystalline superparamagnetic iron oxide nanoparticles (SPION) in a silica matrix. J Alloys Compd. 2012;525:28–33.

25. Balk M, Haus T, Band J, Unterweger H, Schreiber E, Friedrich RP, et al. Cellular SPION Uptake and Toxicity in Various Head and Neck Cancer Cell Lines. Nanomaterials. 2021;11:726.

26. Kokubo T, Takadama H. How useful is SBF in predicting in vivo bone bioactivity? Biomaterials. 2006;27:2907–15.

27. Campion CR, Ball SL, Clarke DL, Hing KA. Microstructure and chemistry affects apatite nucleation on calcium phosphate bone graft substitutes. J Mater Sci Mater Med. 2013;24:597–610.

28. Darroudi M, Hakimi M, Goodarzi E, Kazemi Oskuee R. Superparamagnetic iron oxide nanoparticles (SPIONs): Green preparation, characterization and their cytotoxicity effects. Ceram Int. 2014;40:14641–5.

29. Ma X, Gong A, Chen B, Zheng J, Chen T, Shen Z, et al. Exploring a new SPION-based MRI contrast agent with excellent water-dispersibility, high specificity to cancer cells and strong MR imaging efficacy. Colloids Surf B Biointerfaces. 2015;126:44–9.

30. Shagholani H, Ghoreishi SM, Mousazadeh M. Improvement of interaction between PVA and chitosan via magnetite nanoparticles for drug delivery application. Int J Biol Macromol. 2015;78:130–6.

31. Loh K-S, Lee Y, Musa A, Salmah A, Zamri I. Use of Fe3O4 Nanoparticles for Enhancement of Biosensor Response to the Herbicide 2,4-Dichlorophenoxyacetic Acid. Sensors. 2008;8:5775–91.

32. Samrot AV, Sahithya CS, Selvarani A J, Purayil SK, Ponnaiah P. A review on synthesis, characterization and potential biological applications of superparamagnetic iron oxide nanoparticles. Curr Res Green Sustain Chem. 2021;4:100042.

33. Zheng K, Dai X, Lu M, Hüser N, Taccardi N, Boccaccini AldoR. Synthesis of copper-containing bioactive glass nanoparticles using a modified Stöber method for biomedical applications. Colloids Surf B Biointerfaces. 2017;150:159–67.

34. Greasley SL, Page SJ, Sirovica S, Chen S, Martin RA, Riveiro A, et al. Controlling particle size in the Stöber process and incorporation of calcium. J Colloid Interface Sci. 2016;469:213–23.

35. Sharma RK, Gaur R, Yadav M, Goswami A, Zbořil R, Gawande MB. An efficient copper-based magnetic nanocatalyst for the fixation of carbon dioxide at atmospheric pressure. Sci Rep. 2018;8:1–12.

36. Vergnaud F, Kesse X, Jacobs A, Perton F, Begin-Colin S, Mertz D, et al. Magnetic bioactive glass nano-heterostructures: a deeper insight into magnetic hyperthermia properties in the scope of bone cancer treatment. Biomater Sci. 2022;10.1039.D2BM00319H.

37. Jayalekshmi AC, Victor SP, Sharma CP. Magnetic and degradable polymer/bioactive glass composite nanoparticles for biomedical applications. Colloids Surf B Biointerfaces. 2013;101:196–204.

38. Wang TW, Wu HC, Wang WR, Lin FH, Lou PJ, Shieh MJ, et al. The development of magnetic degradable DP-Bioglass for hyperthermia cancer therapy. J Biomed Mater Res - Part A. 2007;83:828–37.

39. Dadfar SM, Camozzi D, Darguzyte M, Roemhild K, Varvarà P, Metselaar J, et al. Size-isolation of superparamagnetic iron oxide nanoparticles improves MRI, MPI and hyperthermia performance. J Nanobiotechnology. 2020;18:22.

40. Singh RK, Srinivasan A, Kothiyal GP. Evaluation of CaO–SiO2–P2O5–Na2O–Fe2O3 bioglass-ceramics for hyperthermia application. J Mater Sci Mater Med. 2009;20:147–51.

41. Cacciotti I, Lombardi M, Bianco A, Ravaglioli A, Montanaro L. Sol–gel derived 45S5 bioglass: synthesis, microstructural evolution and thermal behaviour. J Mater Sci Mater Med. 2012;23:1849–66.

42. Dinesh Kumar S, Mohamed Abudhahir K, Selvamurugan N, Vimalraj S, Murugesan R, Srinivasan N, et al. Formulation and biological actions of nano-bioglass ceramic particles doped with Calcarea phosphorica for bone tissue engineering. Mater Sci Eng C. 2018;83:202–9.

43. Boccaccini AR, Chen Q, Lefebvre L, Gremillard L, Chevalier J. Sintering, crystallisation and biodegradation behaviour of Bioglass®-derived glass–ceramics. Faraday Discuss. 2007;136:27.

44. Polymeris GS, Giannoulatou V, Kyriakidou A, Sfampa IK, Theodorou G, Şahiner E, et al. Bioactivity characterization of 45S5 bioglass using TL, OSL and EPR: Comparison with the case of 58S sol-gel bioactive glass. Mater Sci Eng C. 2017;70:673–80.

45. Huang Y-C, Lin T-Y, Huang S-C, Yang T-Y, Shih C-J. Copper-enhanced silver releasing from bimetal-containing bioactive glass (AgCu/80S) elicits antibacterial efficacy against drug-resistant Staphylococcus aureus. J Non-Cryst Solids. 2022;584:121509.

46. Zhang Y, Zhang L, Song X, Gu X, Sun H, Fu C, et al. Synthesis of Superparamagnetic Iron Oxide Nanoparticles Modified with MPEG-PEI via Photochemistry as New MRI Contrast Agent. J Nanomater. Hindawi; 2015;2015:e417389.

47. Paiva AO, Duarte MG, Fernandes MHV, Gil MH, Costa NG. In Vitro studies of bioactive glass/polyhydroxybutyrate composites. Mater Res. ABM, ABC, ABPol; 2006;9:417–23.

48. Alicka M, Sobierajska P, Kornicka K, Wiglusz RJ, Marycz K. Lithium ions (Li+) and nanohydroxyapatite (nHAp) doped with Li+ enhance expression of late osteogenic markers in adipose-derived stem cells. Potential theranostic application of nHAp doped with Li+ and co-doped with europium (III) and samarium (III) ions. Mater Sci Eng C Mater Biol Appl. 2019;99:1257–73.

49. Ramos Guivar JA, Sadrollahi E, Menzel D, Ramos Fernandes EG, López EO, Torres MM, et al. Magnetic, structural and surface properties of functionalized maghemite nanoparticles for copper and lead adsorption. RSC Adv. 2017;7:28763–79.

50. Anghel EM, Petrescu S, Mocioiu OC, Cusu JP, Atkinson I. Influence of Ceria Addition on Crystallization Behavior and Properties of Mesoporous Bioactive Glasses in the SiO2–CaO–P2O5–CeO2 System. Gels. 2022;8:344.

51. Fiume E, Barberi J, Verné E, Baino F. Bioactive Glasses: From Parent 45S5 Composition to Scaffold-Assisted Tissue-Healing Therapies. J Funct Biomater. 2018;9:24.

52. Cañas E, Grünewald A, Detsch R, Orts MJ, Sánchez E, Boccaccini AR. In vitro study of bioactive glass coatings obtained by atmospheric plasma spraying. Bol Soc Esp Cerámica Vidr. Elsevier; 2022;61:42–53.

53. Yu Y, Bacsik Z, Edén M. Contrasting In Vitro Apatite Growth from Bioactive Glass Surfaces with that of Spontaneous Precipitation. Materials. 2018;11:1690.

54. Sahu D, Kannan GM, Tailang M, Vijayaraghavan R. *In Vitro* Cytotoxicity of Nanoparticles: A Comparison between Particle Size and Cell Type. J Nanosci. 2016;2016:1–9.

55. Dey S, Das M, Balla VK. Effect of hydroxyapatite particle size, morphology and crystallinity on proliferation of colon cancer HCT116 cells. Mater Sci Eng C. 2014;39:336–9.

56. Li G, Feng S, Zhou D. Magnetic bioactive glass ceramic in the system CaO–P2O5–SiO2–MgO–CaF2–MnO2–Fe2O3 for hyperthermia treatment of bone tumor. J Mater Sci Mater Med. 2011;22:2197–206.

57. Wu C, Fan W, Zhu Y, Gelinsky M, Chang J, Cuniberti G, et al. Multifunctional magnetic mesoporous bioactive glass scaffolds with a hierarchical pore structure. Acta Biomater. 2011;7:3563–72.

58. Marycz K, Sobierajska P, Roecken M, Kornicka-Garbowska K, Kępska M, Idczak R, et al. Iron oxides nanoparticles (IOs) exposed to magnetic field promote expression of osteogenic markers in osteoblasts through integrin alpha-3 (INTa-3)

activation, inhibits osteoclasts activity and exerts anti-inflammatory action. J Nanobiotechnology. 2020;18:33.

59. Walmsley GG, McArdle A, Tevlin R, Momeni A, Atashroo D, Hu MS, et al. Nanotechnology in bone tissue engineering. Nanomedicine Nanotechnol Biol Med. 2015;11:1253–63.

60. Shi S, Jia J, Guo X, Zhao Y, Liu B, Chen D, et al. Toxicity of iron oxide nanoparticles against osteoblasts. J Nanoparticle Res. 2012;14:1091.

61. J. Wang Y-X, Xuan S, Port M, Idee J-M. Recent Advances in Superparamagnetic Iron Oxide Nanoparticles for Cellular Imaging and Targeted Therapy Research. Curr Pharm Des. 2013;19:6575–93.

62. Kesse X, Adam A, Begin-Colin S, Mertz D, Larquet E, Gacoin T, et al. Elaboration of Superparamagnetic and Bioactive Multicore–Shell Nanoparticles (γ-Fe_2O_3@SiO_2-CaO): A Promising Material for Bone Cancer Treatment. ACS Appl Mater Interfaces. 2020;12:47820–30.